

## Research Article

# Surface Morphology and Electrical Resistivity in Polycrystalline Au/Cu/Si(100) System

T. E. Novelo,<sup>1</sup> G. M. Alonzo-Medina,<sup>2</sup> P. Amézaga-Madrid,<sup>3</sup> and R. D. Maldonado<sup>2</sup>

<sup>1</sup>Universidad Tecnológica Metropolitana, Calle 115 (Circuito Colonias Sur) No. 404 por Calle 50, Santa Rosa, 97279 Mérida, YUC, Mexico

<sup>2</sup>Universidad Anáhuac-Mayab, Carretera Mérida-Progreso Km. 15.5 AP 96-Cordemex, 97310 Mérida, YUC, Mexico

<sup>3</sup>Centro de Investigación en Materiales Avanzados, S.C., Av. Miguel de Cervantes 120, Complejo Industrial Chihuahua, 31109 Chihuahua, CHIH, Mexico

Correspondence should be addressed to T. E. Novelo; [tenovelo@hotmail.com](mailto:tenovelo@hotmail.com)

Received 23 October 2016; Revised 5 January 2017; Accepted 18 January 2017; Published 6 March 2017

Academic Editor: Elena Smolentseva

Copyright © 2017 T. E. Novelo et al. This is an open access article distributed under the Creative Commons Attribution License, which permits unrestricted use, distribution, and reproduction in any medium, provided the original work is properly cited.

This work describes the analysis of morphology and electrical resistivity ( $\rho$ ) obtained in the Au/Cu/Si system. The Au/Cu bilayers were deposited by thermal evaporation technique with thicknesses from 50 to 250 nm on SiO<sub>x</sub>/Si(100) substrates. The Au:Cu concentration ratio of the samples was of 25:75 at%. The bilayers were annealed into a vacuum oven with argon atmosphere at 660 K for one hour. The crystalline structures of AuCu and CuSi alloys were confirmed by X-ray diffraction analysis. The scanning electron microscopy (SEM), the atomic force microscopy (AFM), and the energy dispersive spectroscopy (EDS) were used to study the morphology, final thickness, and the atomic concentration of the alloys formed, respectively. The four-point probe technique was used to measure the electrical resistivity ( $\rho$ ) in the prepared alloys as a function of thickness. The  $\rho$  value was measured and it was numerically compared with the Fuchs–Sondheimer (FS) and the Mayadas–Shatzkes (MS) models of resistivity. Results show values of electrical resistivity between 0.9 and 1.9  $\mu\Omega$ -cm. These values are four times smaller than the values of the AuCu systems reported in literature.

## 1. Introduction

The rapid growth and vast exploitation of modern electronics systems create a strong demand for new and improved electronic circuits, as demonstrated by the amazing progress in the field of ultra-large-scale-integration (ULSI) technology [1]. For ULSI devices, it is crucial that the layers of silicides are very uniform and have a low resistivity and a good thermal stability [2–4]. The phase composition, the phase sequence, the morphology, and the temperatures of silicides formation during the interactions of thin metal films with silicon substrates have been massively explored, with both scientific interest and technological importance [5]. Copper is the fastest diffusing transition metal in Si and diffuses through interstitial sites [1]. On the other hand, the gold can form an appropriate barrier between copper and silicon, because it may penetrate through the silicon without reacting with it and presents a low electrical resistivity 2.35  $\mu\Omega$  cm [6]

for ohmic contacts. On the other hand the system AuCu alloy with 50:50% at. Au has been extensively studied, but there is little evidence regarding the 25:75 Au:Cu concentration.

Moreover, the AuCu alloys are widely used in the electronic industry, catalysis, dentistry, jewelry, thin films, and nanocrystal materials because these alloys exhibit excellent mechanical strength, chemical stability, and processability [7, 8]. The binary AuCu system has been extensively studied as a typical representative of the system with order-disorder transformations that occur in certain concentration areas [9]. The phase diagram of the AuCu alloy is not complex, given that it only has three crystallographic structures in ordered phases at temperature below 410°C [10] where the AuCu<sub>3</sub>, CuAu, and Au<sub>3</sub>Cu structures are formed [11–13]. It is important to mention that flexible electronics require highly ductile materials for technological applications in flexible electronics. It has been studied that thin-film AuCu alloys possess superplasticity properties on flexible substrates [14].

The development of these materials could have technological applications in products that can be deformed and the electronics of the product do not present any failure due to the load to which it is subjected. Some properties, such as the electrical resistivity of a metal thin film, depend of the thickness and preparation conditions. [15–18]. Other works have reported that aluminum, gold, copper, and silver have shown a strong resistivity increase with decreasing film thickness, and the differences in surface roughness of those pure materials are very small [19]. However, the differences in the electron mean free path (EMFP) in aluminum, gold, copper, and silver may contribute to the different resistivity behaviors. The resistivity of ordered CuAuI thin films deposited by thermal interdiffusion has been reported with slight changes with decreasing film thickness [20].

In this work the combined effect of the prepared AuCu alloys and silicides by thermal interdiffusion in the Au/Cu/Si systems on the morphology and the electrical resistivity of the alloys are described.

In a previous work, the study of physical and morphological properties of AuCu binary alloys was performed for the three different concentrations: 25 : 75, 50 : 50, and 75 : 25 at%. of Au : Cu alloy for a constant thickness at a temperature of 693 K [21]. However, in the diffraction pattern obtained for the 25 : 75 at% concentration, it presented the formation of composite materials (copper silences) other than the AuCu<sub>3</sub> alloy. This is why the study is deeper for different thicknesses and at a lower temperature than the one implemented in the first job.

In the present work the diffraction pattern was evaluated at a lower temperature (653 K) according to the Au : Cu binary phase diagram for the atomic concentration of 25 : 75. For this atomic concentration the alloy formed is the AuCu<sub>3</sub> [22].

## 2. Experimental Procedures and Techniques

Substrates of 10 × 10 mm<sup>2</sup> size were cleaned with soap, rinsed with distilled water, and dried with air. The p-type silicon substrates (100) were sequential and ultrasonically cleaned with solutions of trichloroethylene, acetone, and isopropyl alcohol for five minutes for each one. Copper films (99.999% purity) were deposited on the silicon substrates by thermal evaporation into a vacuum chamber at 10<sup>-5</sup> Torr. Gold films (99.999% purity) were subsequently deposited on the Cu films forming a bilayer. The film thicknesses were monitored and measured with a quartz crystal sensor through a Maxtek TM-400 controller. Tungsten crucibles were used for metals evaporation. The deposition rate was maintained at 3 Å/s during films deposition. The native silicon oxide layer (SiO<sub>x</sub>) on the surface of substrate was not removed.

The samples were prepared with the Au : Cu concentration of 25 : 75 at.%. The total thickness of each bilayer changed from 50 to 250 nm. The thickness value of each layer was calculated for the selected concentration, by considering the mass density, and the molecular weight of gold and copper, respectively. The bilayer thickness values of each metallic layer of the five samples studied are shown in Table 1.

The bilayers were annealed at 660 K for one hour into a homemade vacuum quartz oven with argon flow [23]. The

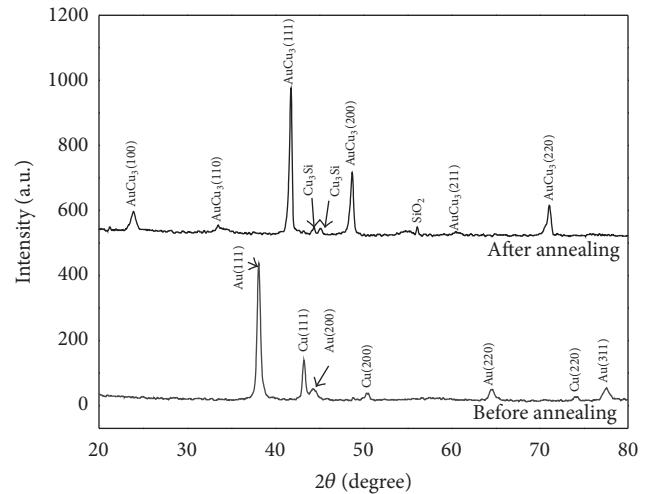


FIGURE 1: DRX pattern for the 250 nm sample before and after the annealing processes.

control of temperature of the vacuum oven was possible by a program developed in LabView software, a HP-6643A System DC power supply, and a HP-3458A multimeter.

The surface morphology of the films was analyzed by atomic force microscopy (Ambios Universal Probe) and by scanning electron microscopy (JEOL 7600F, SEM) techniques. X-ray diffraction (Siemens D-5000) technique at grazing incidence was used to verify the crystalline structure of the formed alloys. Energy dispersive spectroscopy (EDS) was used for determining the stoichiometry of the obtained alloys. The electrical resistivity of the films was measured before and after thermal treatment by the collinear four-probe technique with a Jandel head interconnected with a HP-6443A power supply and a HP-3458A voltmeter of high resolution.

## 3. Results and Discussions

**3.1. DRX Results.** Figure 1 shows the evolution in the crystalline structure of the samples before and after the annealing process. DRX reflects structural changes in the Au/Cu/Si(100) system. Figure 1 shows XRD results for the Au/Cu bilayer before and after the diffusion treatment for the alloy using grazing incidence angle. Two main peaks of the AuCu<sub>3</sub> alloy can be clearly observed (111) and (200) [24]. Thus, the interdiffusion between copper and gold was confirmed where an intermetallic compound was formed instead of the original bilayer before annealing. Figure 1 also shows the main peak (111) of the formed AuCu alloy and the XRD of the Au/Cu bilayer after annealing, corresponding to a stable and cubic structure.

The main peaks of gold and copper are presented in the Au/Cu system of 100 nm total thickness on silicon before annealing; in this diffractogram, they do not show any trace of the other reflection lines of the substrate. After the annealing process, the samples presented the AuCu<sub>3</sub> and Cu<sub>3</sub>Si phases, as it is shown in Figure 1, where the reaction of the substrate with the copper exists; however, there is a

TABLE I: Principal features and deposition parameters of samples analyzed in this work. The thickness (nm), deposition rate ( $\text{\AA}/s$ ), and RMS roughness (nm) are also included.

Sample	Au : Cu (at.%)	Deposition rate ( $\text{\AA}/s$ )	Cu thickness (nm)	Au thickness (nm)	Bilayer thickness (nm)	$T_a$ (K)	Annealing time (h)	RMS roughness (nm)
A	25 : 75	3	34	16	50	660	1	0.9257
B	25 : 75	3	68	32	100	660	1	4.1952
C	25 : 75	3	101	49	150	660	1	5.1907
D	25 : 75	3	135	65	200	660	1	9.1413
E	25 : 75	3	169	81	250	660	1	9.8804

formation of a copper-gold corresponding to the deposited amount. The AuCu<sub>3</sub> phase obtained corresponds to the 25 : 75 at.% of the gold-copper phase diagram (see Figure 1). These results are in agreement with the atomic concentration of the Au/Cu bilayers before the annealing treatment. After the annealing treatment, diffraction peaks corresponding to Cu<sub>3</sub>Si copper silicides were observed. This result reveals the polycrystalline structure resulting from the interaction between the Cu layer and the Si substrate, as a result of the thermal treatment. Some authors have reported that copper is a material with high solubility in silicon, such that its solubility at 500°C is  $1.2 \times 10^{14} \text{ cm}^{-3}$  [25]. This allows the fast diffusion of copper through interstitial sites. A solid-state reaction between Cu and Si occurs already at 200°C in order to form the orthorhombic Cu<sub>3</sub>Si silicide, which is stable at room temperature [26].

Blazevic et al. [27] reported that when thermal treatments are carried out above 400°C, the formation of copper silicides for temperatures of 523 K is proliferated; that is to say, the formation of the intermetallic compound is obtained for the temperature of 653 K.

Iaiche et al. [28] reported in similar Au/Cu/Si systems a high diffusion of Cu in Si by thermal evaporation at 400°C for 30 minutes in vacuum, forming only the Cu<sub>3</sub>Si and Cu<sub>4</sub>Si phases. In the present work we proposed a longer annealing time than other works, in order to achieve the AuCu alloy formation. Some works of Cu/Si contacts [5] report that the phase Cu<sub>3</sub>Si started to be formed from the temperatures close to 170°C. However, with silicon substrates, the reaction begins at 125°C [29]. It is known that the formation of SiO<sub>2</sub> oxide layer in the Cu/Cu<sub>3</sub>Si/Si system at low temperature occurs at the expense of the Cu<sub>3</sub>Si compound [30]. Now the reported reactions are carried out at low temperatures; in our system we work at a higher temperature, so possibly the combination of the alloy formed and the time with the working temperature causes the samples to enter stress and causes a slight shift towards greater angles in the alloys. In summary, it is possible that recrystallization occurs on the surface of the material by modifying crystallographic orientations due to the coalescence or growth of some surface grains and movement of material towards preferential zones as a result of a chemical potential gradient.

**3.2. Morphology.** The surface morphology of Au/Cu/Si(100) sample is shown in Figure 2(a). Mark A on Figure 2(a) indicates the surface of sample and Figure 2(b) shows the EDS results where we can observe a certain concentration of (marks A and B). Found oxygen percentage is probably due to native oxide of silicon. In Figure 2, the formation of an intermetallic compound is observed; it indicates the growth of well-oriented crystallites on the gray background (see mark B), which is mainly composed of silicon (28.42 at.%) provided from substrate. Thus, the growth of well-oriented crystallites on the gray background, which is mainly composed of silicon coming from substrate, has been reported [6, 28]. The rectangular ( $8 \times 5 \mu\text{m}^2$ ) geometries are composed of an AuCu layer with a composition of 47.96 at.% Cu and 15.42 at.% Au (atomic ratio Au : Cu maintaining on 25 : 75 at.% or 1 : 3) diffused with silicon.

Figure 2(c) shows the AuCu bilayer as deposited on silicon before the annealing treatment, and it shows a difference of 2% in the atomic ratio and the initial bilayer of 115 nm. Figure 2(d) shows the bilayer diffused and continued with an average final thickness of 97 nm. All the samples were measured with a decrease of approximately 15% of thickness. This reduction in thickness may be interacting with a rearrangement of material on the surface of the samples probably due to the combined effect of bulk and grain boundaries diffusion.

Figure 3 shows the AFM images with scanning area of  $3 \times 3 \mu\text{m}^2$ , for the alloys obtained in tapping mode at atmospheric pressure for the five samples evaluated. The corresponding roughness value is also reported in Table 1. Samples containing a mixture of two alloys present an increase in roughness and larger grains increased thickness on the surface are observed (see Figure 3(c)).

The statistical grain size results analyzed from the AFM images are shown in Figure 4. In this figure an increasing trend could be seen as the thickness increases. Statistical analysis of AFM images showed a wide range of dispersion in all samples. It is possibly due to the effects of diffusion on the grains causing various grain size distributions where an increase in the standard deviation is derived, which increases as the thickness increases. The average grain size is calculated from the digital AFM matrix of local heights, by means of the computational methods based on the identification of local minimum and saddle points of these local heights, each one defined as a surface grain contour point. From this procedure, we obtained the contour maps of the AFM images. The lateral grain size is defined as the maximum distance between the intersections of the grain's contours in the "x" and "y" directions [31]. Although the thickness is under the surface structures generated by diffusion effects they present larger sizes from the point of view of an area or plant size of these structures. In this case the grain size (lateral size) is not related to the crystallite size or vertical grain size. González-González et al. have conducted an exhaustive discussion of grain size types in thin metal films [32].

The size of the error bars, in Figure 4, is due to the dispersion found in the lateral grain size for each thickness analyzed. There are areas where the material accumulates and others where there is little concentration of material. The samples with smaller thickness have a distribution of lateral grain sizes of the order of the sample error bars with the thickness of 250 nm; this can be attributed to a diffusion effect in the grain boundaries and the diffusion in bulk, generating a large standard deviation in the size distributions of lateral grain. When the thickness increases, there is a major rearrangement or agglutination of material in certain zones generated by the types of diffusion, previously generated probably by gradients of superficial chemical potential.

**3.3. Electrical Resistivity ( $\rho$ ).** Figure 5 shows the  $\rho$  values with the increase of the real thickness measured on the films surface before and after annealing. The samples were measured on surface by the collinear four-probe technique in different zones in order to show the changes on  $\rho$  after annealing treatment. The  $\rho$  values obtained in the initial bilayer can be considered as a mixture of the experimental



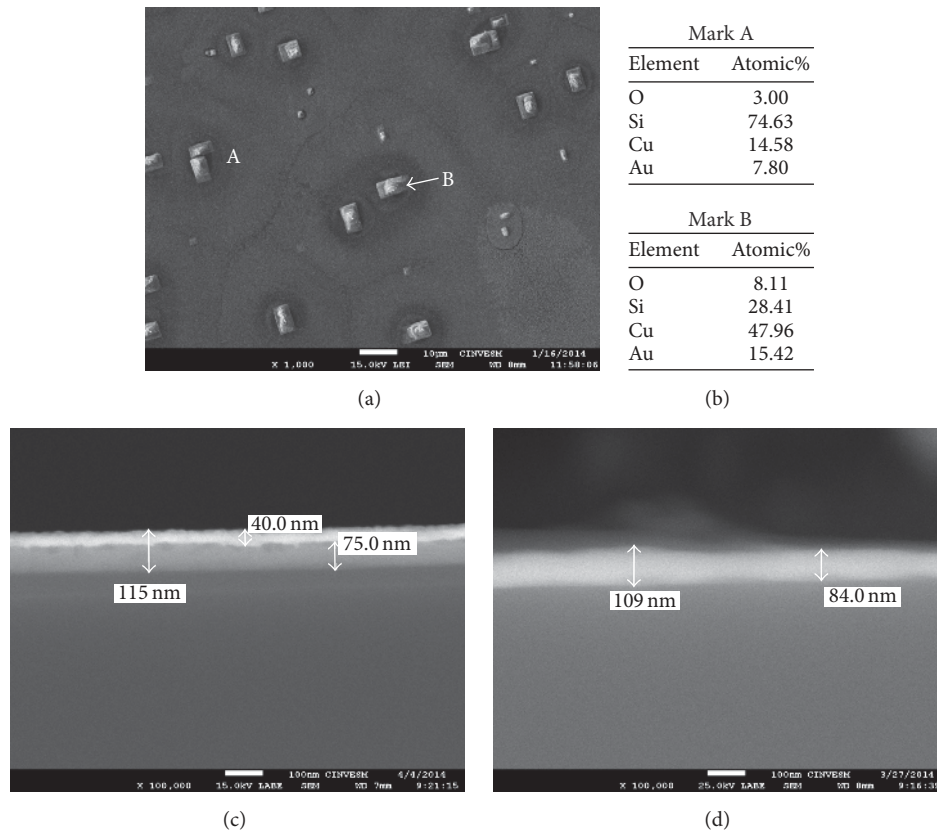


FIGURE 2: SEM images and EDS analysis for the sample of 100 nm thickness. (a) SEM superficial images at 1000x for the annealed sample, (b) EDS analysis of the A and B zones, (c) cross-sectional SEM images at 100000x before annealing, and (d) cross-sectional SEM images at 100000x after annealing treatment.

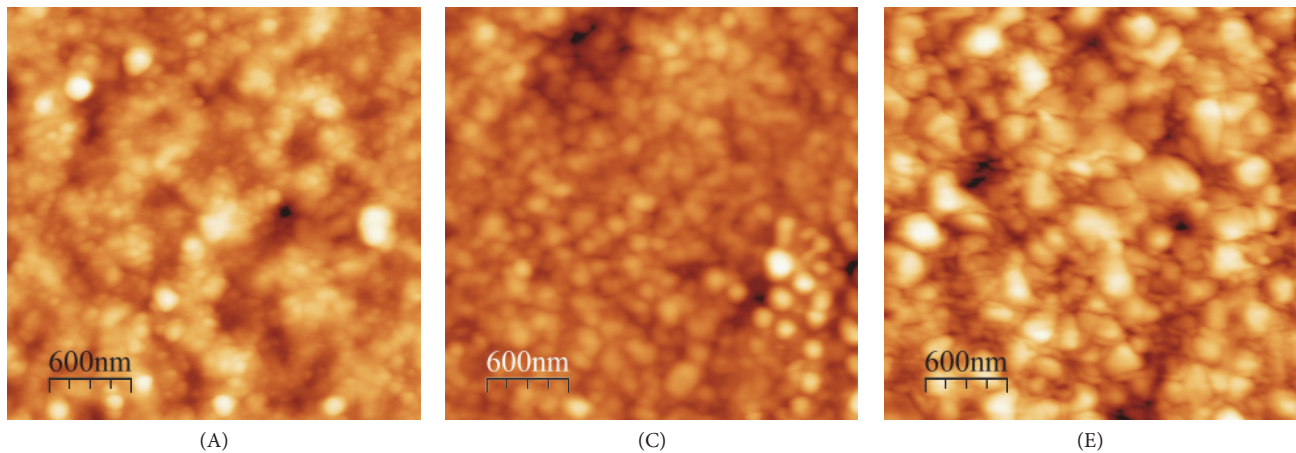


FIGURE 3: AFM images of the alloys (samples A, C, and E) after 1 h of thermal diffusion. Bilayer thickness: 50, 150, and 250 nm, respectively.

measurements of copper and gold (1.67 and 2.66  $\mu\Omega$ -cm bulk value, resp.). When film thickness decreases,  $\rho$  of such films first increases slowly in a first place; this is the typical behavior of the electrical resistivity in thin films. After annealing, a decrement of resistivity was found in annealed samples.

Zhang et al. had reported higher resistivity (7.7  $\mu\Omega$ -cm) in CuAu I alloys in thin films, between 50 and 200 nm approximately [33]. These values tend to be constant between

these thicknesses. Indeed, with decreasing film thickness, the resistivity of films before annealing changed only slightly (see Figure 5). By contrast,  $\rho$  of pure copper and gold after being annealed at 350°C increased dramatically, when the film thickness is approaching the electron mean free paths 39 and 38 nm for copper and gold at room temperature, respectively [34]. The results of our study show a clear decrease in the values of resistivity. This is possibly due to the combination

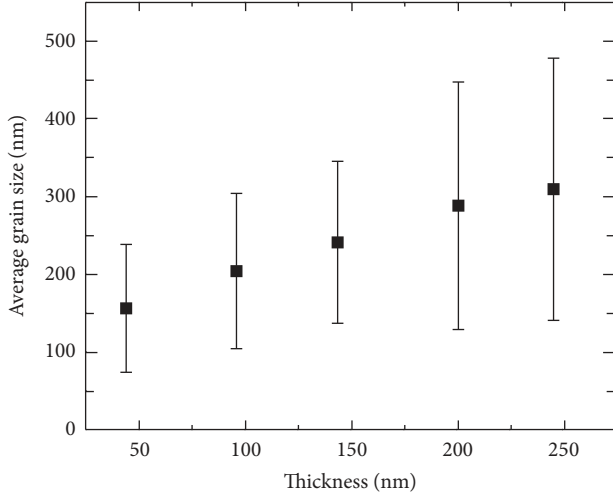


FIGURE 4: Average grain size for the five different samples.

of the AuCu and CuSi alloys. For the behavior reported in the alloys of AuCu, these do not have ranks similar to those we have handled. However, as we increase the thickness, there is a slight increase of  $\rho$ , which could be attributed to the fact that a large amount of material moves towards preferential areas and the diffusion of grain boundaries is more pronounced, as a result of the increasing in the thickness (see Figure 3(c)).

An inverse relationship between film thickness and electrical resistivity has been commonly demonstrated by FS surface scattering and MS grain boundary scattering models. According to the FS model [35, 36], the electrical resistivity in thin film is given for the following equation:

$$\rho = \rho_{\text{bulk}} \left[ 1 - \frac{3}{2k} (1-p) \int_1^{\infty} \left( \frac{1}{t^3} - \frac{1}{t^5} \right) \frac{1 - e^{-kt}}{1 - pe^{-kt}} dt \right]^{-1}, \quad (1)$$

$$k = \frac{d}{\lambda_0},$$

where  $d$  is the film thickness,  $\lambda_0$  is the electron mean free path, and  $p$  is the surface scattering factor. When scattering is totally diffuse (inelastic),  $p = 0$ .

Figure 6 shows the numerical calculations of FS model using the electrical resistivity values of copper in bulk. We decided to use the copper values in the numerical simulation and comparison with the experimental data samples prepared, because the bilayer and nanoalloys have major atomic concentration of copper and electrical resistivity. On the other side the copper film plays an important role in the formation of the two alloys found in the study presented. These values were calculated with different  $p$  and compared with the experimental values measured after the annealing process. It is desirable that experimental resistivity values remain constant for a good approximation to the simulated value; however, as explained above, perhaps this is due to the movement of material generated on the surface of the

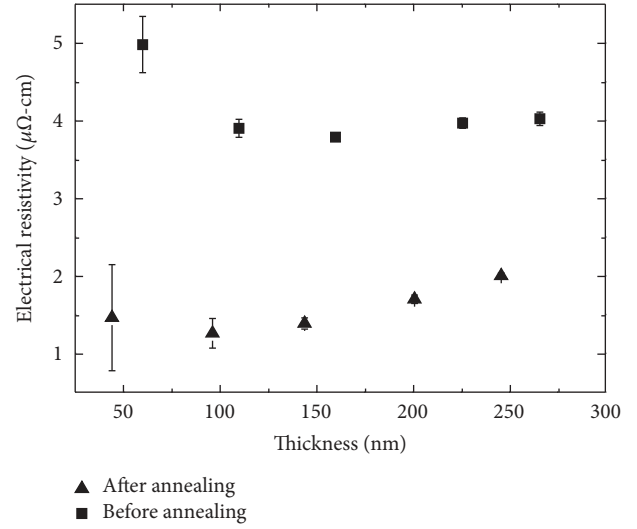


FIGURE 5: Electrical resistivity before and after annealing.

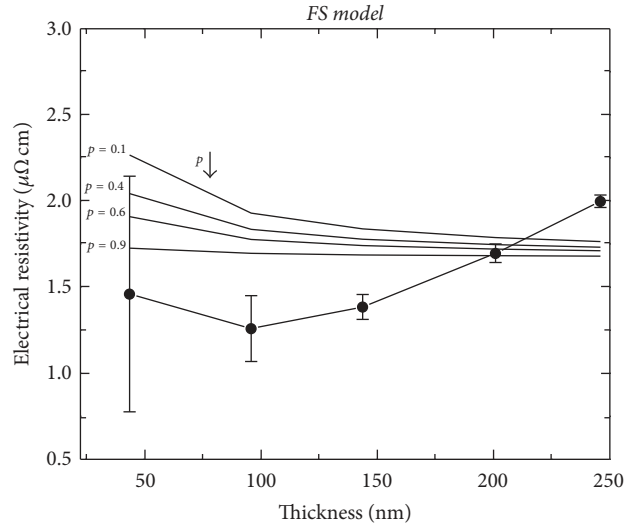


FIGURE 6: Calculated resistivity of Cu by FS model with experimental result of alloys after annealing.

samples given by the diffusion along, which increases the film thickness. Despite all of this, some agreement of the simulated data of FS model with experimental thickness values measured from the cross-sectional images acquired by SEM and implemented in the model to estimate the electrical resistivity can be observed.

Mayadas and Shatzkes (MS) showed a better characterization of the electrical resistivity than the FS model and it is included the contribution of the scattering of electrons due to the grain boundaries. They assume great importance grain size material in comparison with the film thickness as an additional cause of electron scattering [37, 38].

The MS model describes a film representing the grain boundaries as the partially reflecting parallel planes perpendicular to the electric field and the planes are placed at a mean difference distance  $D$ . For specular reflection at the sample

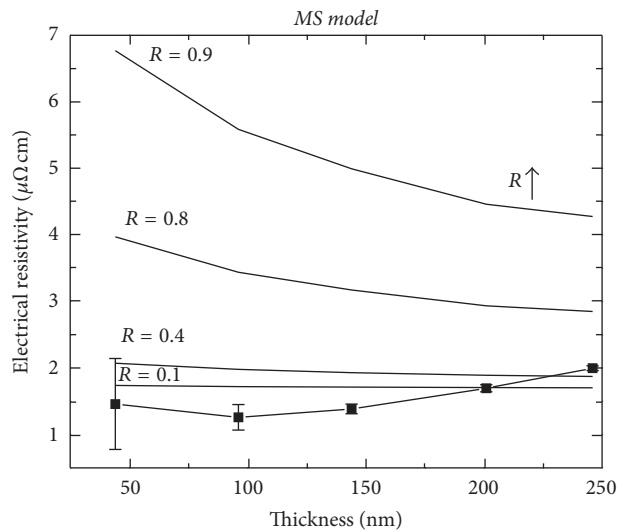


FIGURE 7: Calculated electrical resistivity for Cu using the MS model with experimental result of alloys after annealing.

surface ( $p = 1$ ), the grain boundary enhanced electrical resistivity is

$$\frac{\rho_0}{\rho} = \left[ 1 - \frac{3}{2}\alpha + 3\alpha^2 - 3\alpha^3 \ln\left(1 - \frac{1}{\alpha}\right) \right]^{-1}, \quad (2)$$

$$\alpha = \frac{\lambda_0}{D} \left[ \frac{R}{1-R} \right],$$

where  $R$  is the grain boundary reflection coefficient and  $D$  is the mean grain size width. If  $R = 1$ , electrons are confined to individual grains as they are reflected back at all surfaces.

Similarly to FS analysis, we show, in Figure 7, the comparison between the simulated results of MS model using values of electrical resistivity of Cu in bulk and the grain size values obtained from AFM images. In this comparison, the grain size obtained from statistical analysis of AFM images after the annealing processes is taken into account (Figure 7).

The experimental values compared with the FS model were considered with an approximate value of  $p \approx 0.9$ . This means that the surface is nearly nondispersive. That is, the electrons are reflected in the free surface causing that electrical resistivity to not increase. For the MS model, we used an approximate value of the  $R$  parameter of 0.1. This  $R$  value is less than that calculated value for thin copper films whose value proposed by other authors is  $R = 0.24$  [37, 38]. These results show that the probability that the electrons are reflected in the individual grains is less than reflected in all the surface material. These two parameters analyzed set the stage to confirm that both the surface and the grain boundaries of the material obtained allow the electron to move with less difficulty on the material and this gives results in a low value of electrical resistivity. Comparing both models, the MS model fits better to the experimental results than FS model. The contribution of scattering effect by grain boundaries is more significant than surface scattering in studied sample.

## 4. Conclusions

We have shown that, for systems of Au/Cu/Si(100), the AuCu<sub>3</sub> and Cu<sub>3</sub>Si, alloy gold-copper and copper silicides, respectively, are formed. Annealing by one hour around 390°C leads to the well-oriented growth of crystallites corresponding to Cu<sub>3</sub>Si silicides. The five deposited bilayers were measured before and after heat treatment; the relationship between copper and gold bilayers was 25:75 at.% and the thickness obtained after annealing showed a decrease of 10–15% of original deposited bilayer. Electrical resistivity in surface of the samples was measured and it presented values four times smaller than similar works of the AuCu alloy in thin films. Moreover, their behavior tends to be stable, which is consistent with working for alloys made by thermal diffusion. FS and MS models are implemented and compared with experimental measurements of electrical resistivity, where an approximation of the physical parameters  $p$  and  $R$  of the nanostructured alloys is estimated, and showed appreciable agreement with established models. The implemented and applied studies to any of the FS and MS models methodology allow obtaining physical parameters of the material from electrical and morphological measurements of the samples.

## Competing Interests

The authors declare that they have no competing interests.

## Acknowledgments

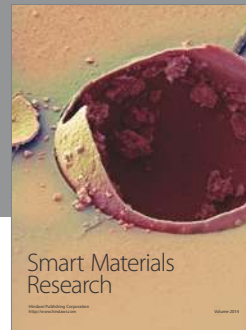
This work was supported by CONACYT (Mexico) through Basic Science Fund 131795 and GIRE Project no. 235637. The authors thank LANNBIO CINVESTAV-Merida, with financial support from CONACYT, FOMIX-Yucatán, and CINVESTAV. The authors thank D. Aguilar, J. E. Corona, D. Huerta, and M. Romero from CINVESTAV-Merida and C. E. Ornelas-Gutiérrez, O. Solis-Canto, E. Torres-Moye, and W. Antunez-Flores from CIMAV-Chihuahua for their technical support.

## References

- [1] Y. Shacham-Diamand, T. Osaka, M. Datta, and T. Ohba, *Advanced Nanoscale ULSI Interconnects: Fundamentals and Applications*, Springer, New York, NY, USA, 2009.
- [2] K. Barmak, C. Michaelsen, and G. Lucadamo, "Reactive phase formation in sputter-deposited Ni/Al multilayer thin films," *Journal of Materials Research*, vol. 12, no. 1, pp. 133–146, 1997.
- [3] R. Pretorius and J. W. Mayer, "Silicide formation by concentration controlled phase selection," *Journal of Applied Physics*, vol. 81, no. 5, pp. 2448–2450, 1997.
- [4] S. P. Murarka, *Silicides for VLSI Application*, Academic Press, London, UK, 1983.
- [5] C.-A. Chang, "Deposition of (100) Au, Ag, Pd, Pt, and Fe on (100) Si using different metal seed layers," *Journal of Vacuum Science and Technology A: Vacuum, Surfaces and Films*, vol. 9, no. 1, pp. 98–101, 1991.
- [6] C. Benazzouz, N. Benouattas, S. Iaiche, and A. Bouabellou, "Study of diffusion at surface of multilayered Cu/Au films on monocrystalline silicon," *Nuclear Instruments and Methods in*

- Physics Research, Section B: Beam Interactions with Materials and Atoms*, vol. 213, pp. 519–522, 2004.
- [7] A. Y. Volkov, “Structure and mechanical properties of CuAu and CuAuPd ordered alloys,” *Gold Bulletin*, vol. 37, no. 3-4, pp. 208–215, 2004.
  - [8] F.-X. Yu, Y.-Q. Xie, Y.-Z. Nie, X.-B. Li, H.-J. Peng, and H.-J. Tao, “Electronic structure of Au-Cu alloys,” *Transactions of Nonferrous Metals Society of China*, vol. 14, no. 6, pp. 1041–1049, 2004.
  - [9] I. Marković, S. Nestorović, and D. Marković, “Effect of thermo-mechanical treatment on properties improvement and microstructure changes in copper-gold alloy,” *Materials and Design*, vol. 53, pp. 137–144, 2014.
  - [10] H. Okamoto, D. J. Chakrabarti, D. E. Laughlin, and T. B. Massalski, “The Au–Cu (Gold-Copper) system,” *Bulletin of Alloy Phase Diagrams*, vol. 8, pp. 455–473, 1987.
  - [11] C. E. Lekka, N. Bernstein, M. J. Mehl, and D. A. Papaconstantopoulos, “Electronic structure of the  $\text{Cu}_3\text{Au}(1\ 1\ 1)$  surface,” *Applied Surface Science*, vol. 219, no. 1-2, pp. 158–166, 2003.
  - [12] Y. S. Puzyrev, G. E. Ice, C. J. Sparks, and L. Robertson, “Automated software for the recovery of the short range order parameters from diffuse X-ray scattering data,” *Nuclear Instruments and Methods in Physics Research Section A: Accelerators, Spectrometers, Detectors and Associated Equipment*, vol. 582, no. 1, pp. 193–195, 2007.
  - [13] A. I. Potekaev, E. A. Dudnik, M. D. Starostenkov, and V. V. Kulagina, “Thermoactivated structure rearrangements in a binary CuAu<sub>3</sub> alloy under deviation from stoichiometric composition,” *Russian Physics Journal*, vol. 53, no. 5, pp. 465–479, 2010.
  - [14] J. Lohmiller, N. C. Woo, and R. Spolenak, “Microstructure–property relationship in highly ductile Au–Cu thin films for flexible electronics,” *Materials Science and Engineering: A*, vol. 527, no. 29-30, pp. 7731–7740, 2010.
  - [15] M. Ohring, *Materials science of thin films*, Academic Press, Second edition, 2002.
  - [16] G. M. Alonzo-Medina and A. I. Oliva, “An in situ technique to measure gold resistance oscillations during the first stages of growth,” *Microelectronics Journal*, vol. 38, no. 3, pp. 388–391, 2007.
  - [17] A. Bid, A. Bora, and A. K. Raychaudhuri, “Temperature dependence of the resistance of metallic nanowires of diameter  $\geq 15$  nm: applicability of Bloch-Grüneisen theorem,” *Physical Review B*, vol. 74, no. 3, Article ID 035426, 8 pages, 2006.
  - [18] R. D. Maldonado, A. I. Oliva, and H. G. Riveros, “Physical properties obtained from measured thermal profiles in the film/substrate bimaterial system,” *Surface Review and Letters*, vol. 13, no. 5, pp. 557–565, 2006.
  - [19] J. M. Camacho and A. I. Oliva, “Surface and grain boundary contributions in the electrical resistivity of metallic nanofilms,” *Thin Solid Films*, vol. 515, no. 4, pp. 1881–1885, 2006.
  - [20] W. Zhang, S. H. Brongersma, O. Richard et al., “Influence of the electron mean free path on the resistivity of thin metal films,” *Microelectronic Engineering*, vol. 76, no. 1–4, pp. 146–152, 2004.
  - [21] T. E. Novelo, P. Amézaga-Madrid, R. D. Maldonado, A. I. Oliva, and G. M. Alonzo-Medina, “Synthesis and characterization in AuCu-Si nanostructures,” *Materials Characterization*, vol. 101, pp. 83–89, 2015.
  - [22] I. Marković, S. Nestorović, and D. Marković, “Effect of thermo-mechanical treatment on properties improvement and microstructure changes in copper-gold alloy,” *Materials and Design*, vol. 53, pp. 137–144, 2014.
  - [23] J. E. Corona, R. D. Maldonado, and A. I. Oliva, “Vacuum oven to control the annealing process in alloyed nanolayers,” *Revista Mexicana de Física*, vol. 53, pp. 318–322, 2007.
  - [24] JCPDS-International Centre for Diffraction Data, Standard Reference 35-1357, 2000.
  - [25] E. R. Weber, *Properties of Silicon*, Institution of Electrical Engineers NSPEC, London, UK, 1988.
  - [26] L. Stolt, A. Charai, F. M. D’Heurle, P. M. Frver, and J. M. E. Harper, “Formation of  $\text{Cu}_3\text{Si}$  and its catalytic effect on silicon oxidation at room temperature,” *Journal of Vacuum Science and Technology A: Vacuum, Surfaces and Films*, vol. 9, no. 3, pp. 1501–1505, 1991.
  - [27] A. Blazevec, H. S. Effenberger, and K. W. Richter, “Phase equilibria in the system Au-Cu-Si and structural characterization of the new compound  $\text{Au}_{5\pm x}\text{Cu}_{2\pm x}\text{Si}$ ,” *Intermetallics*, vol. 46, pp. 190–198, 2014.
  - [28] S. Iaiche, N. Benouattas, A. Bouabellou, L. Osmani, and L. Salik, “Atomic diffusion at the Cu–Au–Si multilayers interface,” *Microelectronic Engineering*, vol. 81, no. 2-4, pp. 349–352, 2005.
  - [29] M. Hanbücken, J. J. Métois, P. Mathiez, and F. Salvan, “Combined AES, LEED, SEM and TEM characterizations of CuSi(100) interfaces,” *Surface Science*, vol. 162, no. 1–3, pp. 622–627, 1985.
  - [30] J. Li, H. Yonezawa, and T. Shigematsu, “Study of low-temperature oxidation in Au/Si and Cu/Si systems by 7-MeV alpha particle backscattering analysis,” *Japanese Journal of Applied Physics*, vol. 31, no. 3, pp. 210–213, 1992.
  - [31] G. M. Alonzo-Medina, A. González-González, J. L. Sacedón, A. I. Oliva, and E. Vasco, “Local slope evolution during thermal annealing of polycrystalline Au films,” *Journal of Physics D: Applied Physics*, vol. 45, no. 43, Article ID 435301, 2012.
  - [32] A. González-González, G. M. Alonzo-Medina, A. I. Oliva, C. Polop, J. L. Sacedón, and E. Vasco, “Morphology evolution of thermally annealed polycrystalline thin films,” *Physical Review B—Condensed Matter and Materials Physics*, vol. 84, no. 15, Article ID 155450, 2011.
  - [33] W. Zhang, S. H. Brongersma, O. Richard et al., “Microstructure and resistivity characterization of CuAu I superlattice formed in Cu/Au thin films,” *Journal of Vacuum Science and Technology B: Microelectronics and Nanometer Structures*, vol. 22, no. 6, pp. 2715–2718, 2004.
  - [34] W. Zhang, S. H. Brongersma, T. Clarysse et al., “Surface and grain boundary scattering studied in beveled polycrystalline thin copper films,” *Journal of Vacuum Science and Technology B: Microelectronics and Nanometer Structures*, vol. 22, no. 4, pp. 1830–1833, 2004.
  - [35] K. Fuchs, “The conductivity of thin metallic films according to the electron theory of metals,” *Mathematical Proceedings of the Cambridge Philosophical Society*, vol. 34, no. 1, pp. 100–108, 1938.
  - [36] E. H. Sondheimer, “The mean free path of electrons in metals,” *Advances in Physics*, vol. 1, no. 1, pp. 1–42, 1952.
  - [37] A. F. Mayadas, M. Shatzkes, and J. F. Janak, “Electrical resistivity model for polycrystalline films: the case of specular reflection at external surfaces,” *Applied Physics Letters*, vol. 14, no. 11, pp. 345–347, 1969.
  - [38] A. F. Mayadas and M. Shatzkes, “Electrical-resistivity model for polycrystalline films: the case of arbitrary reflection at external surfaces,” *Physical Review B*, vol. 1, no. 4, pp. 1382–1389, 1970.





**Hindawi**

Submit your manuscripts at  
<https://www.hindawi.com>

